Innovative Systems Design and Engineering
ISSN 2222-1727 (Paper) ISSN 2222-2871 (Online)
Vol.7, No.8, 2016

A Resonant Photoacoustic CO_2 Sensor Based on MID-IR LED and MEMS Microphone Technology Operating at 4.3µm

Lucky A. Ishaku* David Hutson
Institute of Thin Films, Sensors and Imaging, University of the West of Scotland, Paisley PA1 2BE

Abstract
This paper presents work on the development of a MID-IR LED-based photoacoustic (PA) Carbon dioxide (CO_2) sensor. The transducer used is a MEMS microphone and the sensor was operated in the resonant mode, which makes it the first time that this light source and transducer combination are used in this mode for PA gas sensing, as far as the authors know. Optimisation of the sensor's operation in the resonant mode was done using COMSOL Multiphysics to simulate the fundamental resonance frequency of the PA cell and the optimum position for the microphone. The COMSOL Multiphysics and analytical results computed were validated experimentally. Reduction of the inlet and outlet pipes diameter immensely minimized gas flow noise introduced into the PA cell. Cheaper, miniaturised and stand-alone PA sensors can be produced from Mid-IR LEDs and MEMS microphones because they are small in size, inexpensive and consume less power. The importance of this work largely lies in the fact that the huge market demand for this type of sensors could be met by higher volume production at low cost using this technology. Ultimately the work will be an effective contribution to the monitoring and control of carbon emission.
Keywords: Photoacoustic, Mid-IR LED, MEMS microphone, resonance, COMSOL

1.0 Introduction

Carbon dioxide is one of the principal contributors to global warming and air pollution which undeniably are very big issues in our hands today, because they pose immense threat to both the public and the environment. Many sources have shown that concentration of CO_2 in the atmosphere is increasing rapidly or exponentially [1, 28-30], this implies that the problem is increasing in complexity and unless something is done urgently [2] to avert the substantial consequences, more cataclysmic incidences will continue to occur. In order to adequately fight this global problem CO_2 concentration in air must be monitored and controlled. To achieve this, CO_2 sensors that would be used to provide information about CO_2 concentration in the atmosphere are absolutely necessary. It is obvious that there is a great need for reliable, sensitive and low cost CO_2 sensors which will have a huge market potential because of their versatility in terms of applications [3]. In New York on 29th July 2015 PRN Newswire published a report which forecasts that the gas sensor market will rise to $2.32 billion by 2018 at a compound annual growth rate (CAGR) of 5.56% over the period 2014-2020 [4]. The increase could be because of legislations, growing economies [5] and security. This need led to the idea of developing CO_2 sensors using LED-based MID-IR Photoacoustic Spectroscopy (PAS) which will be accurate, reliable, selective and low cost to suit the current market. Now let us look at what photoacoustic (PA) gas sensing is.

When a modulated light is generated with a wavelength corresponding to the characteristic absorption band of the sample gas in a photoacoustic cell, all or a portion of the gas molecules are excited to a higher energy state by the absorption of the radiating light. The non-radiative relaxation or de-excitation of these molecules (colliding with other molecules and transforming their acquired energy into translational energy) causes increase in temperature and hence pressure of the gas. The temperature and pressure will be modulated because the irradiating light is modulated. This modulated pressure will result in an acoustic wave which can be detected with a sound transducer [5-10], in this case a MEMS microphone. This phenomenon is known as the photoacoustic effect. The increased pressure is directly proportional to the gas concentration which makes it easy for sensor instrumentation [6] and the electrical signal for further processing is produced by the microphone. Figure (1) was generated online from Spectra Calculator; it shows the absorption of CO_2 in the infrared region of 4.26µm which is equivalent to 2347.42cm^{-1} in wavenumber. This is because CO_2 has a strong infrared absorption spectrum around that wavelength. The length, pressure and temperature of the cell were 4cm, 1013.25mbar and 296K respectively in the HITRAN 2004 line list. Carbon dioxide volume mixing ratio (VMR) was fixed at 0.0005.
The acoustic signal generated when heat H(r, t) is produced by the absorption of light by the gas sample can be represented by the lossless inhomogeneous wave equation [7]:

$$\nabla^2 p - \frac{1}{c^2}.\frac{\partial^2 p}{\partial t^2} = \left[\frac{\gamma-1}{c^2}\right].\frac{\partial H}{\partial t} \quad (1)$$

Where p is the acoustic pressure, c is the velocity of sound and $\gamma = c_p/c_v$is the specific heat ratio or adiabatic constant of the gas. This equation is loss free because it does not include the viscous and thermal losses. Taking the Fourier transform of equation (1) gives

$$\left(\nabla^2 + \frac{\omega^2}{c^2}\right) p(r,\omega) = \left[\frac{\gamma-1}{c^2}\right] i\omega H(r,\omega) \quad (2)$$

And

$$p(r,t) = \int p(r,\omega)e^{-i\omega t}d\omega \quad (3)$$

$$H(r,t) = \int H(r,\omega)e^{-i\omega t}d\omega \quad (4)$$

Equation (1) can be solved by taking the time Fourier transform on both sides and expressing the solution $p(r,t)$ as an infinite series expansion of the normal mode solution $p_j(r,t)$ of the homogenous wave equation which are determined by the boundary conditions [7]. The walls of the PA cell are assumed to be rigid, implying that the normal derivative of the pressure is zero at the walls or boundary. This is described by equation (5) [8]:

$$\frac{\partial p}{\partial n} = 0 \quad (5)$$

The four main parts of the sensor are light source, PA cell, acoustic transducer and signal processing and display unit. Getting the PA cell to operate in the resonant mode amplifies the signal and a good quality MEMS microphone with high sensitivity, resolution and noise immunity will produce PA signals of high quality. Resonant mode of operation entails modulating the light emitting diode (LED) at a frequency that coincides with one of the eigenfrequencies of the PA cell while the non-resonant operation mode is achieved by making the LED modulation frequency much less than the eigenfrequencies of the cell. In the latter technique sound is not propagated and standing waves are not formed because the cell dimensions are much smaller than the sound wavelength [9].

One major significance of this research is that the light source (LED) used has not found widespread applications in gas detection yet. Based on the results obtained from some work that have been done with IR LEDs, the authors of [10] forecast that LEDs have the potential to prevail in photoacoustics as light sources. LEDs are small in size, have low power consumption [6] and inexpensive which makes them very convenient for use in sensor miniaturisation. They can be modulated at high frequency by pulsing their currents to as high as in the MHz range and because of the stability of their output power in that range, LED modulation frequency are chosen for PA system optimisation [5].

Some areas where Photoacoustic Spectroscopy (PAS) has found significant applications are environmental pollution monitoring, medical or health diagnostic, the field of life science, detection of gas leakage [11], process control, maintenance, detection of sports performance enhancements substances, security and safety from combustible and toxic substances [5].

2.0 Sensor Design

The photoacoustic cell of the sensor was initially designed to have an acoustic resonator with length 4cm and diameter 1.4cm. Attached to the two open ends of the resonator are two buffer volumes having equal lengths and diameters of 2cm and 4.8cm respectively. These buffer volumes are quarter wavelength of the resonance frequency and at that optimum length there is maximum destructive interference of the standing acoustic noise introduced into the buffers [12]. A buffer volume is considered as an acoustic filter in PA cell design. The transducer which is a microphone is placed at the middle of the resonator because for a cylindrical pipe with both ends open that is where the antinode exists as shown in figure (2). The diagrams in figures (3) and (4) show the PA cell and its dimensions.

A smaller resonator radius would give a higher gas absorption signal. However, radius smaller than 2mm would produce higher background noise owing to the absorption of the beam's Gaussian wings striking the wall of the resonator. The optimum ratio of the radius of the buffer volume to resonator's radius has been found to be approximately 3, given by $r_{buffer} = 3r_{resonator}$. This is because the PA signal is virtually not affected beyond this value [13].

For a cylindrical resonator with both ends open the eigenfrequencies are given by

$$f_j = \frac{\omega_j}{2\pi} = \frac{c}{2}\sqrt{\left[\frac{k}{L}\right]^2 + \left[\frac{\alpha_{mn}}{R_c}\right]^2} \quad (6)$$

Where k represents the longitudinal, m the azimuthal and n the radial modes. For only longitudinal modes m=n=0 and equation (6) becomes

$$f_k = \frac{kc}{2L} \quad (7)$$

Again k is the longitudinal number of harmonics, c is the speed of sound and L is the length of the resonator. The expression for the fundamental resonant frequency was used to calculate f_1 as shown below.

$$f_1 = \frac{c}{2L} = \frac{343}{2 * 0.04} = 4287.5Hz$$

Now considering the effect of acoustic impedance change of $0.6R$ slightly outside the open ends of the resonator known as the end correction [9], the effective length of the resonator is $L + 2 * 0.6R$. For this designed resonator the effective length is

$$L_{eff} = 0.04 + 2(0.6 * 0.007) = 0.0484m$$

Using this effective length changes the fundamental resonant frequency to

$$f_1 = \frac{343}{2 * 0.0484} = 3543.4Hz$$

To calculate the length of the buffer volume the equation for a quarter wavelength pipe was rearranged and applied.

$$L_{buffer} = \frac{c}{4f_1} = \frac{343}{4 * 4287.5} = 0.02m = 2cm$$

In PA sensor design low frequencies are avoided because microphone, amplifier and ambient noise have $1/f$ frequency dependence [14]. The use of modulation frequency in the kHz region has been favourably stated in [9], and the rationale is that the lower limit of the frequency is bounded by $1/f$ noise explained earlier. Practically, this lower boundary is around 1 kHz [11]. On the hand, the upper limit is determined by the operating range of the microphone [11], which is 10 kHz in this design. Modulation frequency range of 1 – 5 kHz should give resonator lengths between 3.4 to 17 cm [14] when equation (1) is used. Frequencies lower than 1 kHz would give resonator lengths longer than 17 cm and this implies that there would be higher influence of $1/f$ noise. Validation of the lower boundary of the resonance frequency was done experimentally. The MEMS microphone SUP01410HR5H-PB has the dynamic range 0 – 10 kHz as shown in figure (5).

A plot of the microphone output signal against frequency in the laboratory shows that ambient noise dominates from 0 Hz to the region close to 1 kHz. It can be seen in figure (6) that from approximately 1 kHz – 10 kHz the microphone frequency response is relatively flat. This is one of the main features of a good microphone [16].

It is therefore recommended that modulation frequencies lower than 1 kHz should not be used because of the high level of noise signal present in that frequency range.

2.1 Analysis of the Fundamental Resonant Frequency

Construction of the PA cell was done by applying all the design parameters explained above and used to carry out measurements in the laboratory. Besides, the resonant frequencies of the resonator were modelled using COMSOL Multiphysics. These modelling were done by using the default COMSOL setting of density of air and the speed of sound in air. The same procedure was repeated but using the speed of sound in CO_2 and its density. The analytical, modelled and experimental results obtained are tabulated as shown in table (1).

These results show very good agreement and confirm that using the effective length for calculation and modelling is the best approach, because it gives results that have little discrepancy with experimental work. For normal length there is a significant difference of over 700 Hz between analytical/COMSOL and experimental results, indicating that the use of normal length of the resonator for analytical or modelling work should be avoided. The results presented in table 2 were obtained by employing only the effective length, since it has been shown to be the optimum length for both analytical and modelling work.

All the methods have shown a shift in the fundamental resonance frequency from about 3.5 kHz in air to approximately 2.8 kHz in 100% CO_2. This is in line with the fact that temperature and the composition of gases change the speed of sound which in turn changes the resonance frequency as shown in equations (8) and (9). In practical applications the change in gas composition will not be as much as 100% and so the resonance frequency too would not drift by a large value. It is important to state that a shift in resonance frequency much less than the half-width at half maximum (HWHM) of the resonance curve would not cause a considerable change in the PA signal [12].

$$c = \sqrt{\frac{\gamma \mathrm{RT}}{\mathrm{M}}} \qquad 8$$

$$f_1 = \frac{c}{2L} = \frac{1}{2L}\sqrt{\frac{\gamma \mathrm{RT}}{\mathrm{M}}} \qquad 9$$

Where R is the ideal gas constant, T is the temperature and M is the molar mass of the gas. Other parameters in these equations have already been defined.

Further experimental frequency analysis in terms of the PA signal showed a change from 3.57 kHz to 3.85 kHz in air when the light source was placed outside the buffer volume. The former resonant frequency was obtained when the source was located close to the open end of the resonator. This shift in resonance frequency is due to coupling of all the gas-filled parts of the acoustic system [17]. Now considering the PA cell as a single unit gives the results in table (3) from both experiments and COMSOL Modelling. This table shows that the difference between experimental and COMSOL results for the two conditions of air and 100% CO2 is roughly around 1 kHz. It also indicates that for a complex PA cell geometry other than the conventional cylindrical shape, there is no straight forward method of computing the resonance frequency analytically.

Figures (7) and (8) are the diagrams of the COMSOL modelled geometry and result respectively. The latter shows the position where the optimum PA Signal can be obtained, which is where the maximum acoustic pressure is propagated. This is the rationale for placing the microphone in the middle of the resonator.

2.2 Quality Factor

Frequency measurements were made around the resonance frequency and plotted in order to calculate the quality factor which is the value by which the output signal is amplified or multiplied. See the graph in figure (9).
The bandwidth, $BW = 0.07kHz$ and the resonance frequency, $f_0 = 3.85kHz$. Therefore the quality factor of the PA cell is:

$$Q = \frac{f_0}{BW} = \frac{3.85}{0.07} = 55$$

3.0 Results and Discussion on the PA signal

Laboratory test results showed that resonance tracking is highly essential in resonant PA Sensors. Measurement of PA signal was carried out without tracking the resonance frequency and the results were plotted as shown in figure (10).

This graph shows that without tracking the resonance frequency the PA signal was low in amplitude (μV) and very unstable. The fluctuation in this mode of operation was high because of the sensitivity of the acoustic system to ambient noise in the laboratory and the system's inability to use the natural amplification of resonance.

Conversely, a resonance tracking circuit was designed for the PA system. Using the same LED as source of radiation in the PA cell, measurements were carried out for increasing concentration of CO_2 buffered by nitrogen in ratios. The range of CO_2 concentration is 0 – 100%. See graph in figure (11).

It can be seen from the graph that the PA signal increases with percentage rise in concentration of CO_2 in the PA cell. This shows that resonance tracking is very important in PA sensors because it tackles the major problem of acoustic resonators in practical applications [17], particularly where there is much change in temperature and the gas composition. A graphical relationship between the resonance frequency and concentration of CO_2 in the resonator is also presented in figure (12).

This graph shows that as the CO_2 concentration increases it lowers the speed of sound which causes a decrease in the resonance frequency in the PA cell. This happens because the molar mass of CO_2 (44 g/mol) is greater than that of N_2(28 g/mol). Equations (8) and (9) show the relationship.

3.1 Effect of Gas Flow Rate Background Signal on the PA Signal

Usually gas flow affects the accuracy and hence the reliability of PA signals. This necessitated running the experiments with LED switched off in one case and the LED left on but covered in the other case. The results obtained were plotted on the same axis with the results shown in figure (11). This comparative plot is presented in figure (13).

The blue graph is the signal generated when the LED (light source) was switched on whereas the red graph is the flow background signal which was measured when the LED was turned off. This background signal is significantly high despite the noise cancellation provided by the buffer volumes at the resonance frequency. Data for the green graph was obtained when the LED was left in the ON position but covered with a thick paper and tape. The LED Off and LED Covered graphs are very identical because there was no infrared radiation to excite the CO_2 molecules. It can be seen from these graphs that there is a sharp increase in the noise signal from the flow rate of about 80 SCCM upward. The dominant effect of this background signal on the PA signal implies that the cell design needs to be improved, most especially the gas inlet and outlet.

3.2 Reduction of the Inlet and Outlet Pipes Diameters

In order to reduce the gas flow background signal the diameter of the inlet and outlet pipes was reduced from 3.8mm to 1.0mm. The same measurement procedures were followed and the results obtained are presented in figure (14).

Reducing the diameters of both the gas inlet and outlet pipes drastically lower the effect of gas flow background signal on the PA signal. At 1mm diameter the background signal is relatively flat up to the maximum range of the measurement (140 SCCM). This means that larger diameters of inlet and outlet pipes should be avoided in order to reduce flow noise. However this comes as a trade-off with the response time of the sensor.

4.0 Conclusion

A photoacoustic CO_2 sensor based on MID-IR LED technology operating in the resonant mode has been successfully developed using a MEMS microphone as the transducer. A notable feature which made this work a success was the resonance frequency tracking which proved to be very essential in situations where there are high changes in temperature and gas composition. The LED's emission spectrum is narrow and has a centre wavelength around 4.2μm for high selectivity. In order to optimize the sensor's operation in this mode, experimental results were used to validate COMSOL simulations and analytical determination of the fundamental resonance frequency of the PA cell. The optimum position of the microphone in the cell was also shown in the pictorial COMSOL simulation result presented. Operating the sensor in resonant mode offers the advantage of natural amplification

and the modulation frequency was chosen to avoid ambient noise which is dependent on 1/f. The results obtained are good indications that LEDs and MEMS microphones are very good light source and transducer combination for PA gas sensing, because of advantages like small size, low power consumption and low cost; features which enhance sensor miniaturisation. Gas flow noise was greatly minimized by the reduction of the gas inlet and outlet pipes diameter; however the sensor system can be improved by designing filters at these inlet and outlet pipes. Besides, further improvements can be done by reducing the resonator diameter and polishing the inside walls of the cell. This is because resonator diameter is inversely proportional to PA signal and plating the walls with gold will reduce parasitic absorption which could produce false PA signal. According to [14] the ratio of length to radius of 1 D longitudinal resonator should be greater than 10:1 so that excitation in the azimuthal mode is avoided and dynamic viscous loss and radiation loss are eliminated. Part of the future design modification can be the replacement of the current LED with one that delivers more power because PA signal is proportional to radiation power. The effect of temperature, pressure and water vapour on the sensor's performance will also be looked into. To the knowledge of the authors of this paper, this is the first time that MID-IR LEDs are used with MEMS microphones in the resonant mode of operation for PA gas sensing.

Acknowledgement
Special thanks to Jim Orr for the mechanical construction of the PA cell from stainless steel. The authors are grateful to Gerry O'Hara for helping out with useful information in the laboratories. Also the provision of the Mid-IR-LED by Gas Sensing Solutions (GSS) is acknowledged with much appreciation.

References

[1] Lee T. J., Kim J., Shterengas L., (2012), "CO2 Sensor with Data Logger System" *Systems, Applications and Technology Conference (LISAT) 2012 IEEE* Long Island.
[2] Shuying M., Yuquan M., Lidong C., Shiguang L., (2010), "Design of a New Measurement and Control System of CO2 for Greenhouse Based on Fuzzy Control" *2010 International Conference on Computer and Communication Technologies in Agriculture Engineering.*
[3] Neethirajan S., Jayas D. S., Saditap S., (2008), "Carbon Dioxide (CO2) Sensors for the Agri-food Industry – A Review" *Food Bioprocess Technol.*
[4] P R Newswire (2015), **"**Global Gas Sensors Market - Growth, Trends & Forecasts (2014-2020)".
[5] MINIGAS Project Report (2011) "Miniaturised photoacoustic gas sensor based on patented interferometric readout and novel photonic integration technologies (MINIGAS)"
[6] Kuusela, T., Peura, J., Matveev B.A., Remennyy M.A., Stus N.M., (2009), "Photoacoustic gas detection using a cantilever microphone and III-V mid-IR LEDs". *Vibrational Spectroscopy Vol51, Issue 2*
[7] Rosencwaig A., (1980), "Photoacoustics and Photoacoustic Spectroscopy". *John Wiley and Sons.*
[8] Baumann B., Kost B., Wolff M., Groninga H., (2008), "Modeling and Numerical Investigation of Photoacoustic Resonators" *Intechopen*
[9] Miklos A., Hess P., Bozoki Z., (2001), "Application of Acoustic Resonator in Photoacoustic Trace Gas Analysis". *Rev. Sci. Instrum. Volume 72, Issue 4*
[10] Bozoki, Z., Pogany, A., and Szabo, G., (2011), "Photoacoustic Instruments for Practical Applications: Present, Potentials, and Future Challenges" *Applied Spectroscopy Reviews, Volume 46, Issue 1, 2011*
[11] Besson J. P., (2006), "Photoacoustic Spectroscopy for Multi-gas Sensing Using Near Infrared Lasers" *A PhD Thesis*
[12] Yang C., Arsad N., Min L., Yao W. (2013), "Buffer Structure Optimization of the Photoacoustic Cell for Trace Gas Detection" *Optoelectronics Letter Volume 9, No. 3*
[13] Bijnen F. G. C., Reuss J., Harren F. J. M. (1996), "Geometrical Optimization of a Longitudinal Resonant Photoacoustic Cell for Sensitive and Fast Trace Gas Detection". *Rev. Sci. Instrum. Volume 67, Issue 8.*
[14] Tavakoli M., Tavakoli A., Taheri M., Saghafifar H. (2009), "Design, Simulation and Structural Optimization of a Longitudinal Acoustic Resonator for Trace Gas Detection Using Laser Photoacoustic Spectroscopy" *Optics and Laser Technology (2010)*
[15] Knowles SiSonic Microphone SPU0141HR5H-PB Product Data Sheet
[16] Peters R. J., Smith B. J., Hollins M., (2010), "Acoustics and Noise Control" 4th Edition. *Pearson Prentice Hall.*
[17] Miklos A., (2015), "Acoustic Aspects of Photoacoustic Signal Generation and Detection in Gases" *International Journal of Thermophysics.*
[18] Ulasevich A. L., Gorelik A. V., Kouzmouk A. A., Starovoitov V. S. (2013), "A Miniaturized Prototype of Resonant Banana-Shaped Photoacoustic Cell for Gas Detection"
[19] Duggen, L., Lopes, N., Willatzen, M., Rubahn, H. G. (2011), "Finite Element Simulation of Photoacoustic Pressure in a Resonant Photoacoustic Cell Using Lossy Boundary Conditions"
[20] Parvitte, B., Risser, C., Vallon, R., Zeninari, V. (2012), "Modelization of Photoacoustic Trace Gases

Sensors" *COMSOL Conference 2012 Milan*
[21] Szakáll, M., Csikós, J., Bozóki, Z., and Szabó, G. (2007), "On the Temperature Dependent Characteristics of a Photoacoustic Water Vapour Detector for Airborne Application". *Infrared Physics and Technology. Volume 51, Issue 2*
[22] Mohebbifar, M.R., Khalilzadeh, J., Dibaee, B., and Parvin, P. (2014), "Effect of Buffer Gases on the Performance of SO2 Trace Measurement Based on Photoacoustic Spectroscopy". *Infrared Physics & Technology Volume 65*
[23] Besson J. P., Schilt S., Thévenaz L., (2004), "Multi-gas sensing based on photoacoustic spectroscopy using tunable laser diodes" *Science Direct*
[24] Koskinen V, Fonsen J, Roth K, Kauppinen J (2008), "Progress In Cantilever Enhanced Photoacoustic Spectroscopy" *Vibrational Spectroscopy Volume 48, Issue 1, 18 September 2008, Pages 16–21*
[25] Angela E., Pietro M. L., Cinzia D. F., and Vincenzo S., (2009), "Photoacoustic Techniques for Trace Gas Sensing Based on Semiconductor Laser Sources" *Sensors (Basel).*
[26] Scholz L., Perez A. O., Knobelspies S., Wollenstaein J., Palzer S. (2015), "MID-IR LED-based, photoacoustic CO2 Sensor" *Procedia Engineering*
[27] Kohring M., Bottger S., Willer U., Schade W. (2015), "LED-Absorption-QEPAS Sensor for Biogas Plants", *Sensors*
[28] Mauer J., "Climate Change 101: CO2 concentration" *Stoneforge Chronicles.*
[29] National Oceanic and Atmospheric Administration (NOAA), "Recent Global CO2 Concentration.
[30] Scripps Institution of Oceanography, "CO2 Concentration from 1700 - Present (Ice - Core data before 1958. Mauna Loa data after 1958)

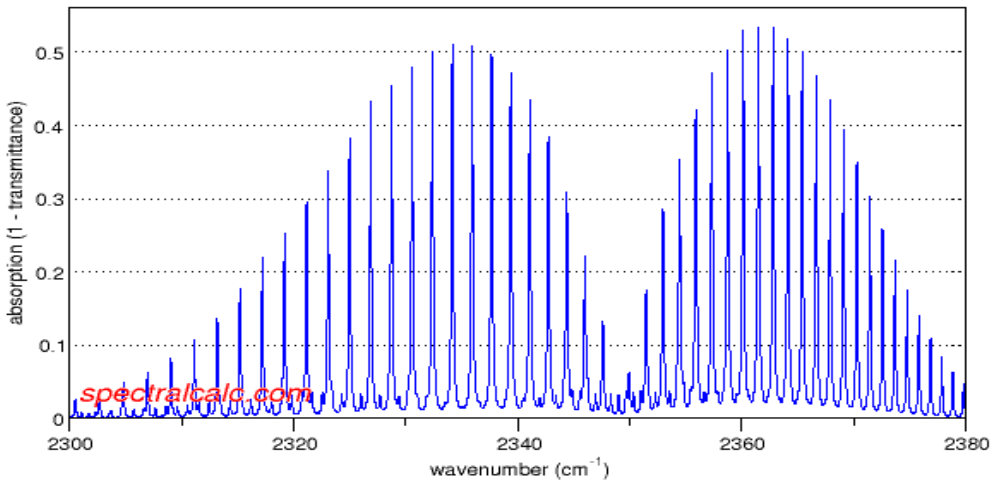

Figure 1: Absorption spectra of CO_2 around 2347.42cm^{-1}, corresponding to 4.26µm.

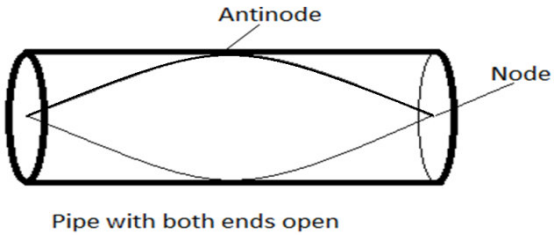

Figure 2: The resonator

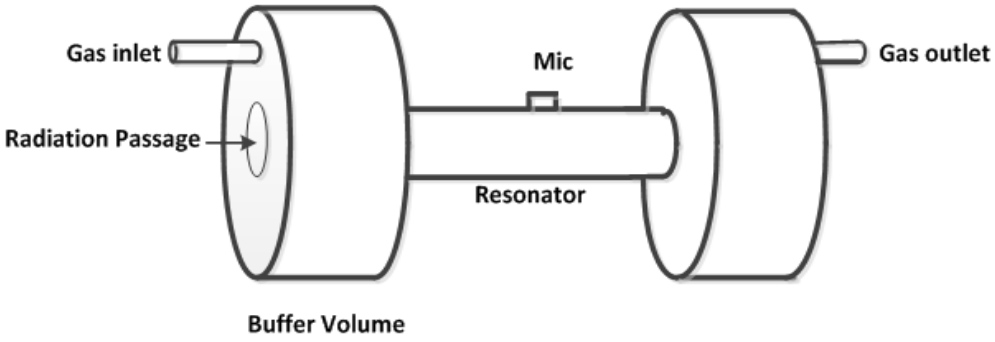

Figure 3: Photoacoustic Cell

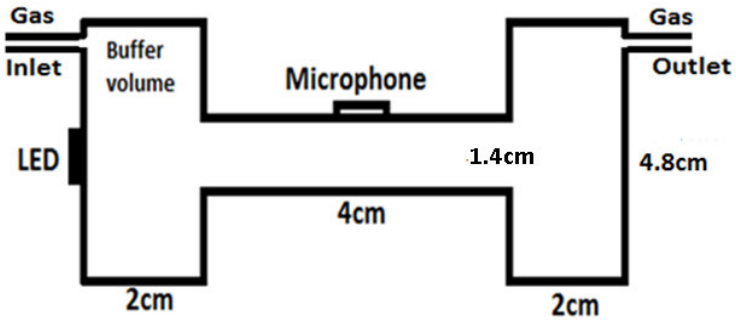

Figure 4: Dimensions of the Initial PA cell

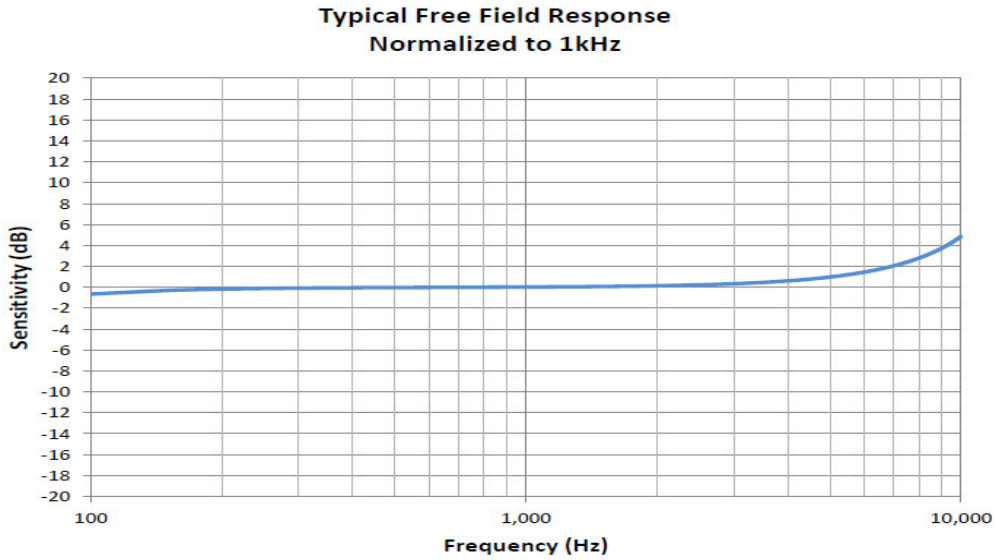

Figure 5: Microphone Frequency Response Curve [15]

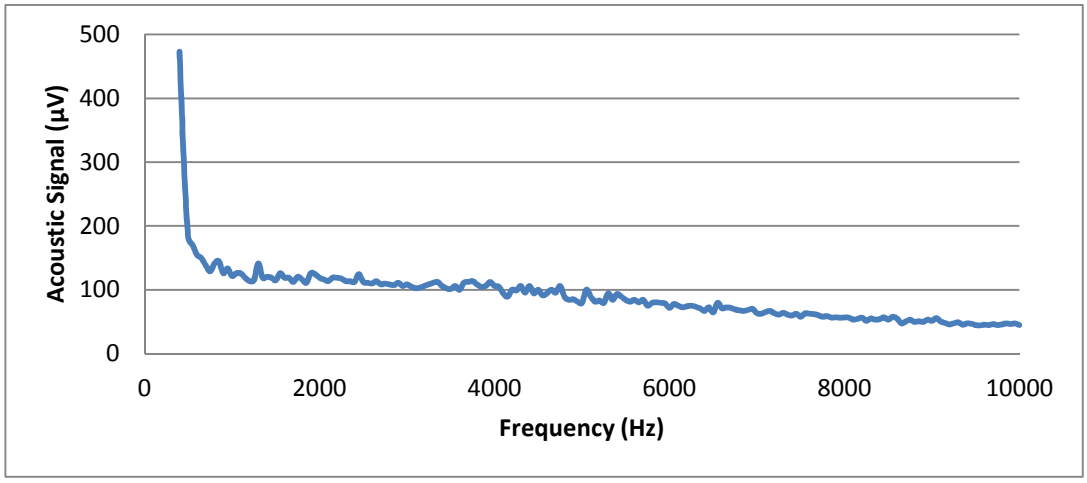

Figure 6: Microphone Frequency Response to Laboratory Ambient Noise

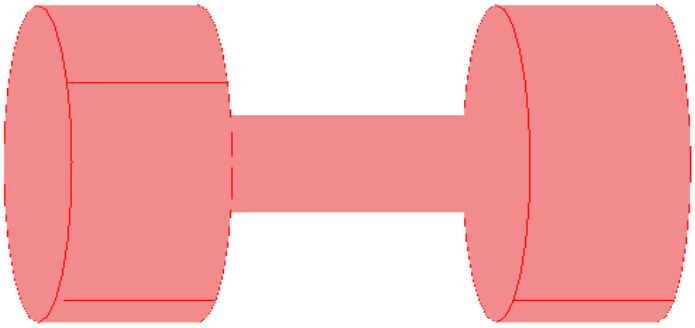

Figure 7: PA cell geometry in COMSOL.

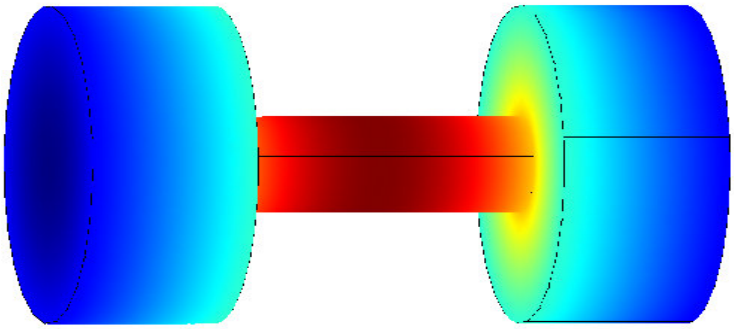

Figure 8: COMSOL modelling result showing position of highest acoustic Signal - RED.

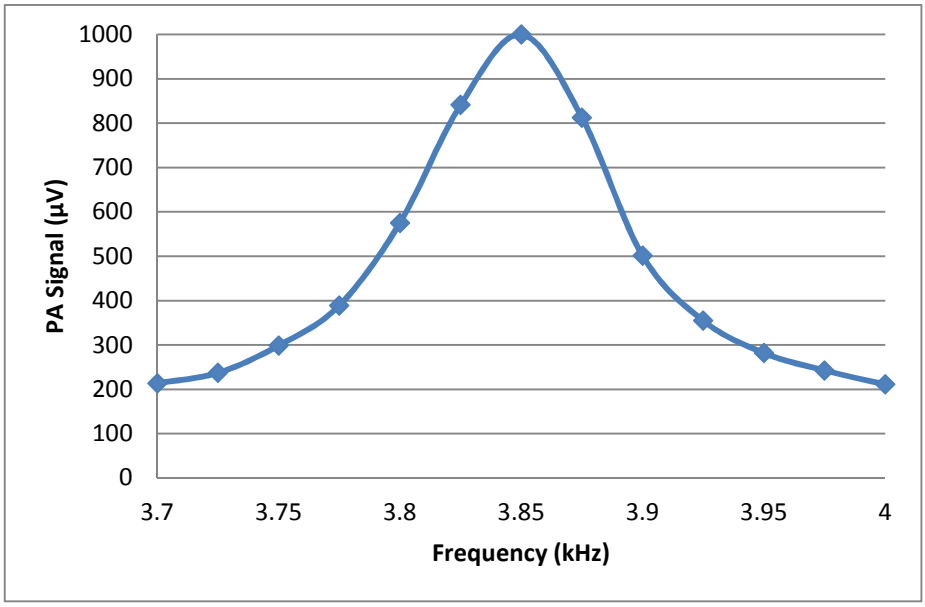

Figure 9: Resonance frequency profile

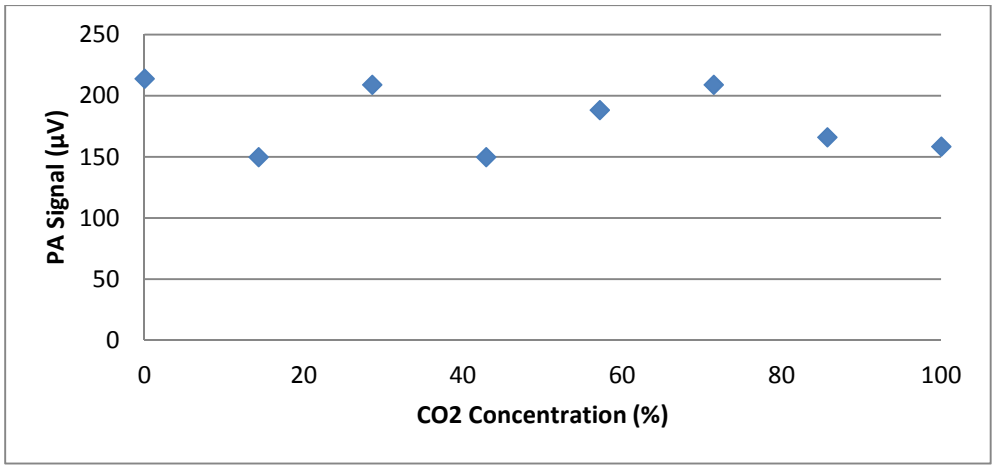

Figure (10): PA signal versus CO2 Concentration (%) without Frequency Tracking

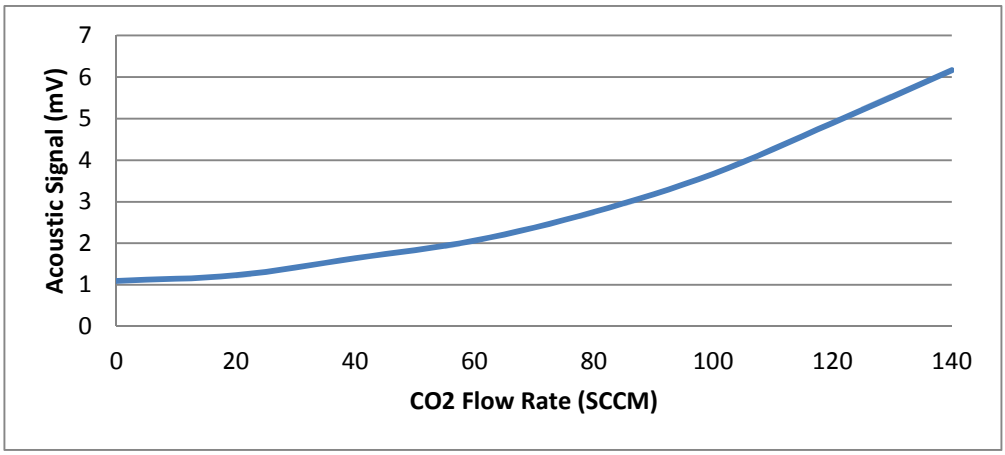

Figure 11: Graph of PA Signal against % concentration of CO_2 in the cell

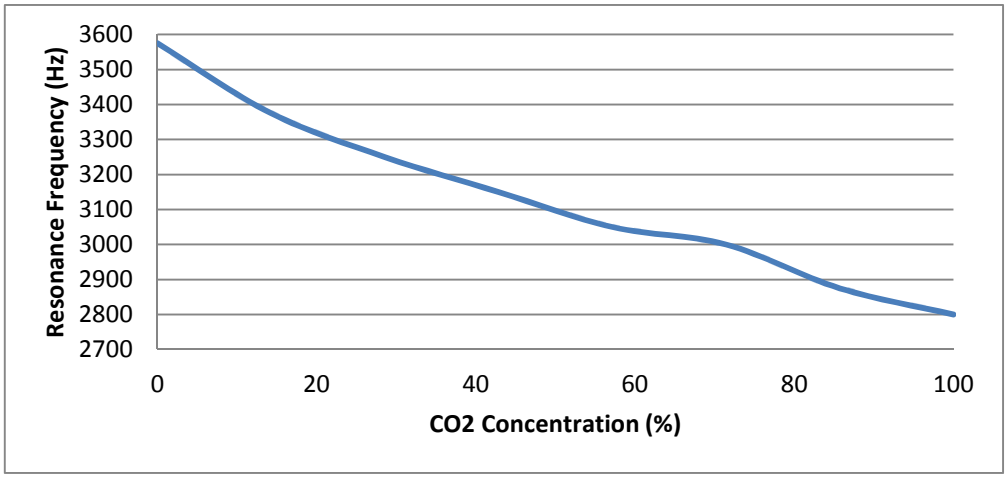

Figure 12: Resonance frequency versus CO_2 concentration plot.

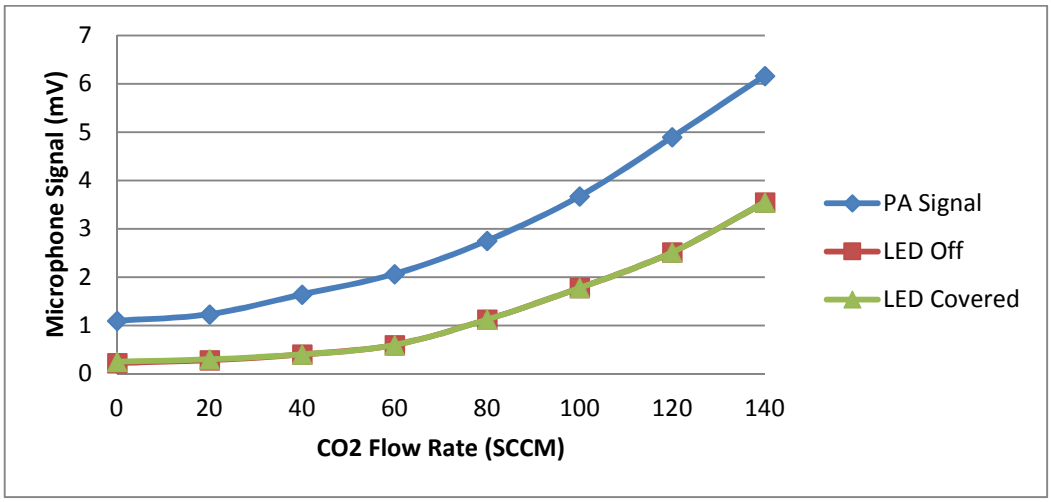

Figure 13: Effect of gas flow background signal on PA signal at inlet diameter of 3.8mm

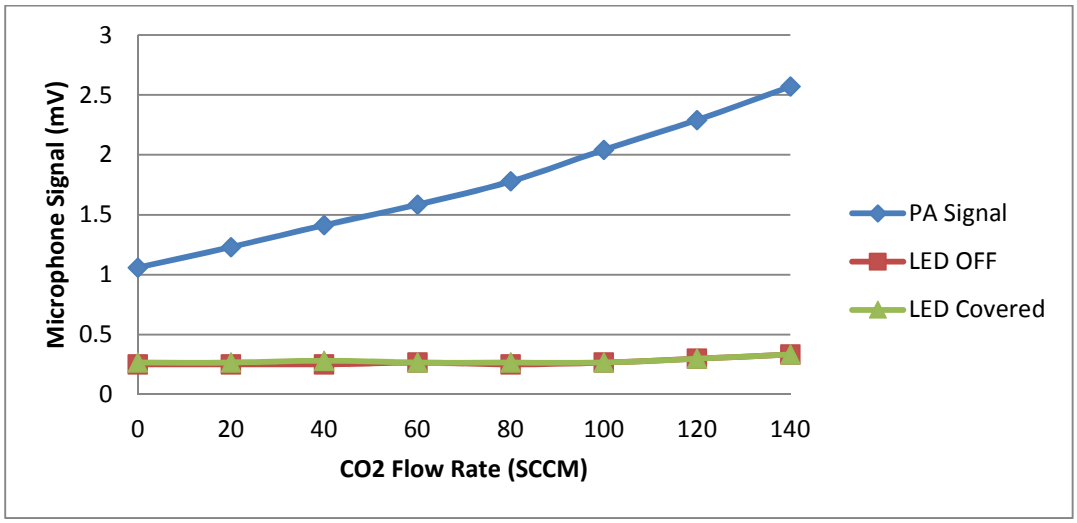

Figure 14: PA Signal and Gas Flow Noise at inlet and outlet pipes diameters of 1.0mm

Table 1: Fundamental Resonant frequencies in *air* for the resonator

Method	Longitudinal Fundamental Frequency (Hz)	Resonator Length Used
Analytical	4287.50	Normal length
COMSOL	4287.47	Normal length
Experimental-loud speaker Signal	3570.00	-
Experimental - PA Signal	3575.00	-
Analytical	3543.40	Effective Length
COMSOL	3543.78	Effective length

Table 2: Fundamental Resonant frequencies for the Resonator in CO_2 Using the Effective length

Method	Longitudinal fundamental frequency in 100% CO_2 (Hz)
Analytical	2758.16
COMSOL	2758.26
Experimental using PA Signal	2800.00

Table 3: Fundamental Resonant Frequencies in CO_2 and Air for the PA Cell (resonator plus buffer volumes)

Method	Longitudinal fundamental frequency in 100% CO_2 (Hz)	Longitudinal fundamental frequency in Air (Hz)
Analytical	-	-
COMSOL	2208.80	2837.76
Experimental using PA Signal	3000.00	3825.00